BULLETIN OF THE EARTHQUAKE
RESEARCH INSTITUTE
Vol. 58 (1983), pp. 385-400

13. An Experimental Study on Mechanism of Implosion Earthquakes during the 1973 Successive Eruptive Activity of Asama Volcano.

By Hiroshi IMAI,

Earthquake Research Institute,
University of Tokyo.

(Received March 25, 1983)

Abstract

In the course of eruptive activity of Asama Volcano in 1973, successive eruptions occurred during the period 16 to 18 February. Implosion earthquakes associated with the eruptive activity were examined by the present author, who presented a model for mechanism of the successive eruptions. A liquid film of magma in the model plays an important role in a discussion on energetics of dynamical process inside a volcanic conduit to interpret earthquake magnitudes of the implosion earthquakes. However, there is little information available for the film thickness of viscous liquid in the model. From this point of view, one of the most basic experiments was carried out to learn this information and to examine the validity of the model. In the present experiment, several kinds of silicon oils, whose viscosities are 50, 100, 300, 500 and 1000 cs, were used on the basis of a parameter N_f which supports the application of the experimental results to the volcanological model. The film thickness was assumed to be one tenth of inner diameter of a volcanic conduit in the model. In the experimental results, the ratio of the film thickness of viscous liquid to the inner radius of pipe was found to range from 0.2 to 0.35 (or 0.1 to 0.18 to the inner diameter). Therefore, the model would be further confirmed from the present experiment. Moreover, a few basic data relative to bubble rising in viscous liquids are also discussed.

1. Introduction

Asama volcano erupted on February 1, 1973, after a quiescence of 11 years. After the first eruption on Feb. 1, 10 major eruptions, five minor eruptions and successive minor eruptions were observed and the eruptive activity ended on May 24 of the same year. Including the precursory

phenomena, SHIMOZURU *et al.* (1975) and WATANABE (1976) investigated the 1973 eruptive activity of the volcano. Many volcanic earthquakes associated with the major or minor eruptions were recorded at the seismic stations of the Asama Volcano Observatory (A.V.O.) and the volcanic earthquakes were analyzed (SHIMOZURU *et al.*, 1975; IMAI *et al.*, 1979; IMAI, 1980, 1982, 1983).

Among the volcanic earthquakes, those termed implosion earthquakes were found during the successive eruptive activity which occurred on Feb. 16 to 18. It was confirmed by the staff of A. V. O. that the earthquakes occurred synchronously at the time when individual minor eruptions took place. Their earthquake magnitudes ranged from 1.0 to 1.6 and their hypocenters were found to be roughly in the depth range of 0.5 to 1.5 km just below the summit crater of the volcano (IMAI, 1982). Initial motions of the implosion earthquakes indicated that certain implosive events may occur in the volcanic body, *e. g.* in a volcanic conduit. Thus, a mechanism of successive eruptions as inferred from the features of seismic data was presented by IMAI (1983), who introduced an idea of two-phase flow system into a discussion of a model for mechanism of successive minor eruptions which took place at the volcano. In the model, the thickness of a liquid film of magma plays an important role in a discussion on the energetics of the dynamical change which occurrs in a volcanic conduit. However, there is little information on the film thickness of viscous liquid available for the energetics.

For the sake of examining the validity of the model of successive eruptions as presented by IMAI (1983), one of the most basic experiments of two-phase flows is carried out. In the experiments, a silicon oil and a bit of air are used as a liquid-phase and a gas-phase, respectively.

2. A model of successive eruption

A brief description of the model for mechanism of successive eruptions is introduced here. The model was presented by IMAI (1983) who introduced the idea of two-phase flows consisting of liquid magma and gas bubbles into the model as shown in Fig. 1. In a volcanic conduit, (a) gas bubbles are produced at the exsolution surface (ES). If water is assumed to be a main volatile component, then the surface is located at the level where a vapor pressure line crosses a hydrostatic pressure line. (b) Bubbles exsolved in magma grow larger gradually by decompressive expansion as the magma rises or the bubbles themselves rise in magma, by coalescence of neighboring bubbles, and by diffusion of dissolved volatiles into bubbles. (c) Such a

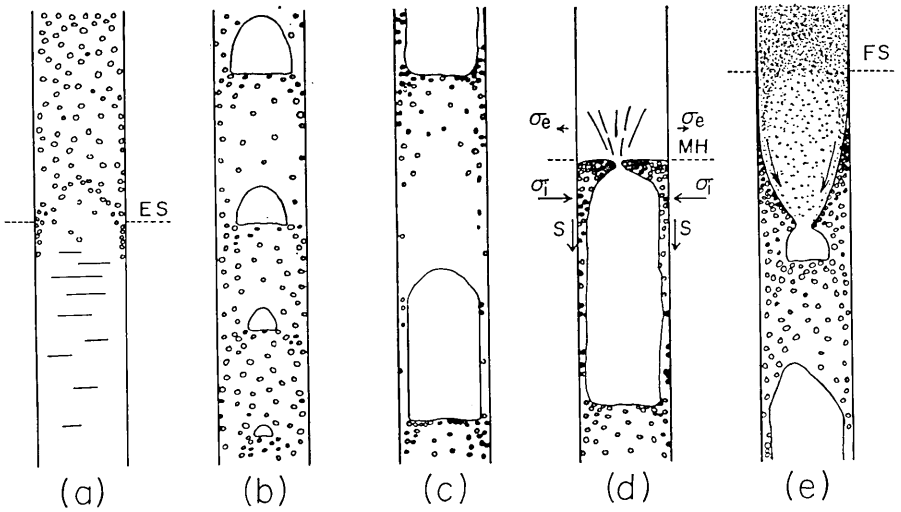

Fig. 1. Schematic illustrations of a process modelled as two-phase flow patterns. ES, MH and FS denote the exsolution surface, the (effective) magma head and the fragmentation surface, respectively. σ_i, σ_e and S denote the normal stress acting inward on the volcanic conduit wall, the normal stress outward on the wall, and the shear stress acting along the wall, respectively. (after IMAI, 1983)

bubbly flow changes into a slug flow which consists of large gas bubbles and the bubbles rise up to the tip of the magma head (MH) where they disrupt. As soon as a disruption occurs, an inward collapse follows within the conduit. These phenomena may be supported by the initial downward or pull motions of earthquakes obtained during the successive eruptive activities of the volcano. Once the disruption occurs, a magma film between the walls of a volcanic conduit and gas bubbles flow down to give the shear stress (S) along the conduit wall and the normal stress (σ_i) caused by the release of gas in bubbles acts on the conduit wall. σ_i should be somewhat greater than the normal stress σ_e caused by the expansion of the released gas. When a down-flow of magma film is realized, an opposite directional shear stress for S as inferred from the principle of action-reaction can be neglected. This is because the down-flow is performed so as to balance between shear stresses acted on a magma film from a conduit wall and acted on a conduit wall by a magma film whose thickness gradually becomes thin. (d) A parcel of gas squeezed out of a bubble flows up with fragments (or drops) of magma and/or fractured conduit wall rocks as an annular flow in which each component moves in its own velocity. Their velocities decrease immediately by their own frictions or due to the conduit wall. Then, they form a gentle eruption cloud which is expanded mainly by

thermal energy.

3. Apparatus

Experimental equipment for the measurement of hydrostatic pressure in the present study is shown in Fig. 2. The pressure sensor is installed on the side of a cylindrical pipe whose inside diameter ($2R$) is 2.0 centimeters. The pressure sensor can detect the hydrostatic pressure at the location of the sensor precisely in the range of 0 to $\pm 0.1\ kg/cm^2$.

An air cavity whose shape is cylindrical horizontally is also installed at the bottom of pipe as shown in Fig. 2 and the air cavity is able to rotate around the center axis as shown.

In the present experiment, several kinds of silicon oils whose viscosities are 50, 100, 300, 500 and 1000 cs (centistokes) are used as liquid-phases in two-phase flow systems. Their physical properties are listed in Table 1.

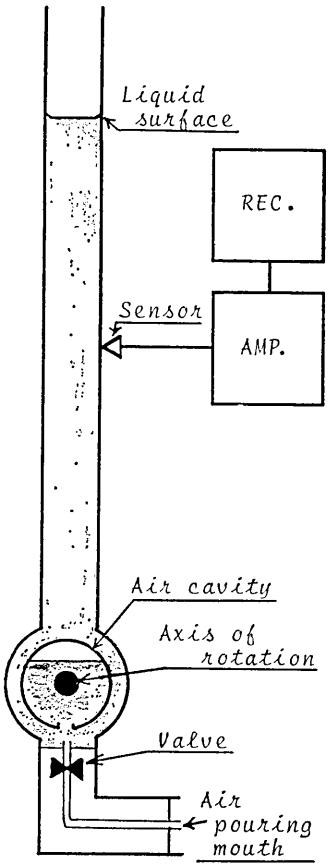

Fig. 2. Mechanical and electrical aparatuses used in the present experiment. A gas bubble is formed by rotating the axis of the air cavity located at the bottom of the cylinderical pipe.

4. Analysis of experimental data

4.1 Method of analysis

As mentioned in the previous section, a certain volume of air is let into an air cavity whose mouth faces downward as seen in Fig. 2. By rotating the axis, the accumulated air is

Table 1. Physical properties of silicon oils at 25°C.

	viscosity (centistokes)				
	50	100	300	500	1000
density (gr/cm^3)	0.955-0.965	0.960-0.970	0.965-0.975	9.965-0.975	0.965-0.975
viscosity (cs)	50±2.5	100±5	300±15	500±25	1000±50
surface tension (dyne/cm)	—	20.9	—	—	—
specific heat (cal/gr°C)	—	0.36	—	—	0.36
heat conductivity (cal/cm·sec·°C)	—	3.7×10^{-4}	—	—	3.8×10^{-4}

released to form a bubble rising inside the pipe. If the bubble is large enough to fill the available flow section of pipe, the bubble is termed "a gas-plug" or "a slug-flow bubble". Hydrostatic pressures, which are associated with the bubble rising, at the location of the pressure sensor are measured continuously in time until a bubble bursts at the liquid surface and up to the recovery of its initial condition from the time when the air was let into the air cavity. A typical profile of the change of hydrostatic

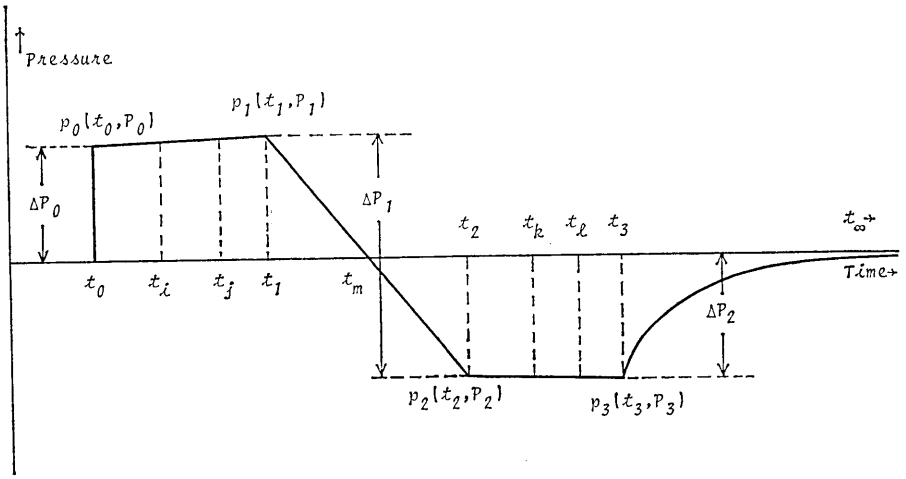

Fig. 3. A typical profile of the change in hydrostatic pressure measured by the pressure sensor installed at a pipe wall.

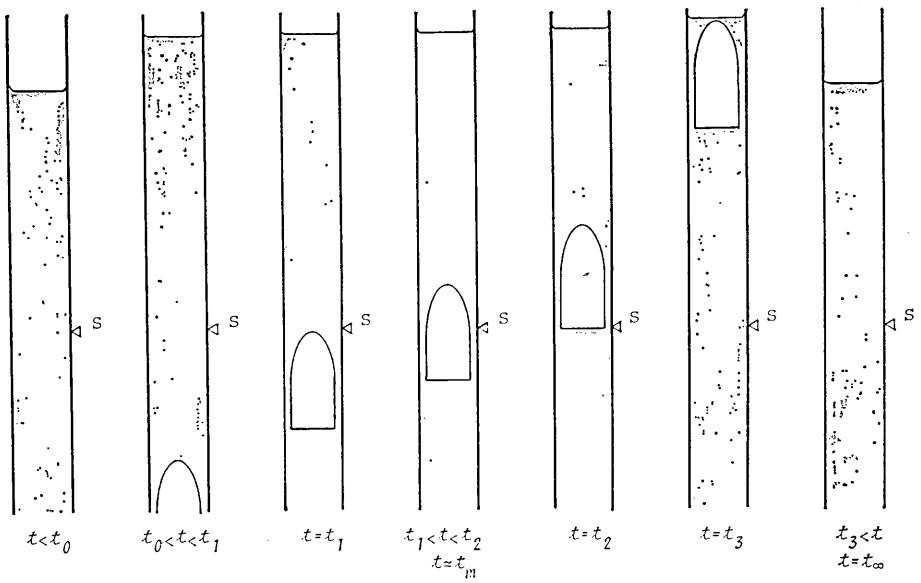

Fig. 4. Locations of bubbles with time sequence corresponding Fig. 3.

pressure obtained in the experiments is shown in Fig. 3. Figure 4 shows the relationship between the locations of the bubble, the pressure sensor and the liquid surface as a function of time. t_0, t_1, t_2, t_3 and t_∞ signify the times when the air let into the air cavity has just started to rise as a gas-plug, the time when the top of bubble has just reached the location of pressure sensor, the time when the bottom of bubble has just reached the location of pressure sensor, the time when the top of bubble has just reached the liquid surface and the bubble is about to burst and the time when the system has recovered to its initial condition before the time t_0, respectively.

When we measure a hydrostrtic pressure in time, we can get the following information :

(a) V_0: *volume of air let into a cavity*

When we let air into the air cavity, we use a medical syringe. When we use it, however, the volume of air can not be measured accurately by use of a scale drawn on a syringe, because of a leak at the connection between the needle and the body of the syringe or for other reasons. The volume of air V_0 is obtained as follows. A certain volume of air is let into the cavity, with the result that the corresponding hydrostatic pressure increases by ΔP_0. Then, we can formulate the equation,

$$\Delta P_0=\rho g \Delta h \,, \tag{1}$$

where Δh is the increase on height of a liquid surface due to the air let in. Therefore, we can get V_0 by

$$V_0=\pi R^2 \Delta P_0/\rho g \,, \tag{2}$$

where R, ρ and g are the inside radius of pipe, the density of a viscous liquid inside the pipe and the gravitational acceleration, respectively

(b) dV/dt: *volumetric expansion rate of a bubble due to its rising.*

As seen in Fig. 3, the pressure increases gradually in time between t_0 and t_1. This is because the hydrostatic pressure on a bubble decreases as the bubble rises. These calculations are carried out only in cases where a bubble exists below the pressure sensor. Assuming that a bubble expands from V to $V+\Delta V$ in the unit time with the result that a liquid surface rises by Δh, then, we have

$$\Delta V=\pi R^2 \Delta h \,.$$

$$\Delta P=\rho g \Delta h \,,$$

where ΔP is the pressure increase due to a liquid surface moving up by Δh. Therefore, we get

$$dV/dt=(\pi R^2/\rho g)(dP/dt)_{01} \,. \tag{3}$$

where the subscript "01" means that the value is available for $t_0<t<t_1$ and $(dP/dt)_{01}$ is just the slope inclination of time-pressure $(t-P)$ curve as shown in Fig. 3. Therefore, we can also write

$$dV/dt=(\pi R^2/\rho g)(P_j-P_i)/(t_j-t_i)\,, \tag{4}$$

where,

$$t_0<t_i<t_j<t_1\,,$$

$$P_0<P_i<P_j<P_1\,,$$

since the $t-P$ curve between the time t_0 and t_1 can be regarded as a straight line.

(c) *v_g: bubble rising velocity*

The hydrostatic pressure P measured at the position of the pressure sensor depends only on the height of liquid column between the tip of a bubble and the liquid surface just while the bubble is passing the side of the pressure sensor. Moreover, the pressure includes the change of pressure associated with a bubble rising and the volumetric expansion of the bubble itself. Therefore, the bubble rising velocity is represented as a function of time. As shown in Fig. 5, when a bubble rises in the vicinity of the pressure sensor, we can get the following equation by means of the similar technique mentioned before:

$$h_b-h_a=[v_g(t_m)+(1/\pi R^2)(dV/dt)](t_b-t_a)\,,$$

where $v_g(t_m)$ is the approximate rising velocity just around the position of the bubble between the times t_a and t_b. If Δh is taken as a plus, we can get

$$-dh/dt=v_g(t_m)+(1/\pi R^2)(dV/dt)\,.$$

Since the first term of the right-hand side in the above equation is 10^2 times the magnitude of the second or over, we can rewrite the above equation approximately as

$$-(dh/dt)_{t=t_m}=v_g(t_m)\,.$$

When we use the relationship between h and P, we get

$$v_g(t_m)=-(1/\rho g)(dP/dt)_{t=t_m}\,. \tag{5}$$

Generally, we write

$$v_g(t_m)=-(1/\rho g)(dP/dt)_{12}\,, \tag{6}$$

where the subscript "12" means that the value is a good aproximation during the times t_1 to t_2. Additionally, the effective length of the bubble just around the pressure sensor is obtained as

$$L(t)_{12}=v_g(t)_{12}\cdot(t_2-t_1) \tag{7}$$

or approximately,

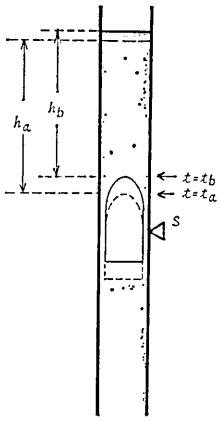

Fig. 5. Schematic illustration of a bubble rising in the vicinity of the pressure sensor. The pressure measured by the sensor is only caused by a liquid column existing aobve the tip of a bubble. The column height of a liquid depends upon the bubble rising velocity and the volumetric expansion rate of a bubble itself due to the decrease of hydrostatic pressure acted on it.

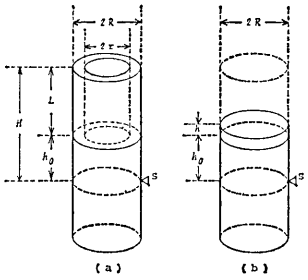

Fig. 6. Schematic model for the calculation of liquid film thickness. Formulations are found in the text.

$$L(t)_{12} \cong \Delta P_1/\rho g\,, \qquad (8)$$

where ΔP_1 is found in Fig. 3.

(d) δ : *film thickness*

The conditions, of the system that a bubble just reaches a liquid surface (see Fig. 4 (f)), and of the system recovered the initial condition after a certain measure of time (see Fig. 4 (g)), are modelled as seen in Fig. 6 (a) and (b). We consider that a liqid film, existing between the pipe wall and the wall of a bubble whose effective length is L, flows down to make a cylinder, whose height is h, clogged up with liquid. Then, the thickness of a liquid film is defined as

$$\delta = R - r\,.$$

We can get

$$h = (1 - r^2/R^2)L\,. \qquad (9)$$

On the other hand, h is represented as

$$h = \Delta P_2/\rho g\,, \qquad (10)$$

where ΔP_2 is seen in Fig. 3. Therefore, we can obtain

$$\delta = R[1 - \{1 - \Delta P_2/\rho g L\}^{1/2}]\,. \qquad (11)$$

We next have to get L. If t_m is taken as $(t_1+t_2)/2$, we can write L as a function of time as follows:

$$L(t) = L(t)_{12} + (1/\pi R^2)(dV/dt)(t - t_m) \qquad (12)$$

or

$$L(t) = L(t)_{12} + (1/\rho g))dP/dt)_{01}(t - t_m)\,. \qquad (13)$$

Using Eq. (11), we can get

$$\delta = R[1-\{1-\Delta P_2/\rho g L(t_3)\}^{1/2}], \tag{14}$$

because L appeared in Fig. 6 or Eq. (11) corresponds to the time t_3 as seen in Fig. 3.

4.2. Results of analysis

Since each run of the present experiment is very reproducible, only one run is sufficient for a certain volume of air and a certain viscosity of silicon oil. Then, the number of runs totalled to 20, 21, 23, 22 and 24, which represent the numbers of changes in volume of air let into the cavity, related to silicon oils whose viscosities are 50, 100, 300, 500, and 1000 cs, respectively. The pressure profiles are obtained as the analogue data. At the time of transforming analogue data into digital data by use of a digitizer with a magnifying glass, however, some inaccuracy due to the parallax in readings is unescapable. Therefore, a datum is read twice and the results due to the procedures mentioned in the previous section are plotted in Figs. 7, 8 and 9.

The volume rate (volumetric expansion rate) of a bubble relative to the initial volume of bubble is shown in Fig. 7. It is found that the lower the viscosity of a liquid, the faster the decompressive expansion of the bubble. On the other feature, the expansion rate of a bubble increases with the initial volume of bubble regardless of liquid viscosity. As seen in Fig. 7, however, these data are widely spread. The cause may be due to the parallax in readings of the data or the mechanical problem on the sensitivity of the data recorded for a very small input voltage.

The rising velocity of a bubble relative to the initial volume of bubble is shown is Fig. 8. The velocity of a bubble increases as the liquid viscosity decreases. The velocity of a larger bubble becomes more stable with an increase of liquid viscosity. On the contrary, the smaller the bubble, the slower the rising velocity.

The dimensionless film thickness between pipe wall and the bubble wall relative to the initial volume of the bubble is shown in Fig. 9. The greater the liquid viscosity, the thicker the liquid film, roughly irrespective of bubble dimension. It should be noted that the film thickness becomes more than 0.3 times the radius of cylindrical pipe for a viscous liquid whose viscosity is more than 300 cs.

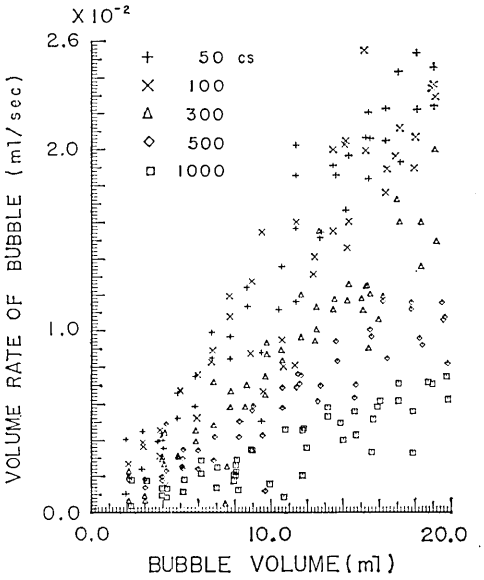

Fig. 7. Experimental result on the volumetric expansion rate of bubble associated with the decrease of hydrostatic pressure acting on the bubble due to its rising in a viscous liquid within a cylindrical pipe.

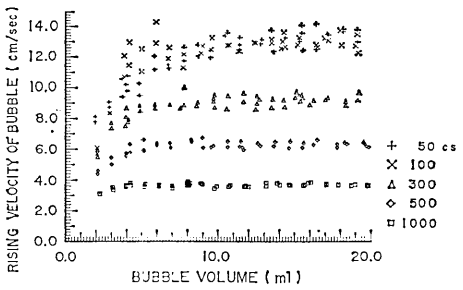

Fig 8. Experimental result on the bubble rising velocity in several kinds of viscous liquid within a cylindrical pipe whose diameter is 2.0 cm.

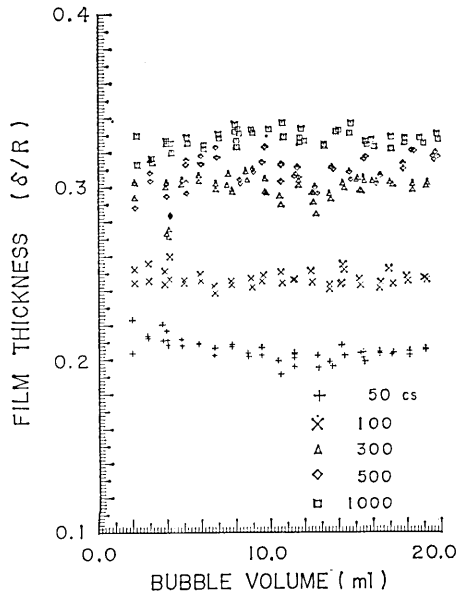

Fig. 9. Experimental result on the liquid film thickness for several kinds of viscous liquid within a cylindrical pipe whose diameter is 2.0 cm. The film thickness is represented dimensionlessly by the raio of an actual film thickness to the inner radius of pipe.

5. Application of experimental results to the mechanism of successive minor eruptions

In this paper, the argument shall be progressed according to WALLIS (1969). WALLIS (1969) introduced the dimensionless inverse viscosity N_f in order to arrange the experimental data of two-phase flows. In this section, we examine the rising velocity of a single bubble in a stagnant and viscous liquid.

Three cases are considered for the dynamics of flow based on the government of flow patterns. The cases are termed the inertia dominant, the viscosity dominant and the surface tension dominant cases, respectively (WALLIS, 1969). The surface tension dominant cases are not discussed, because in such cases the bubble does not move at all. In the following section the density of air ρ_g is negligible as against the density of liquid ρ_f, because $\rho_g \ll \rho_f$ can be assumed. In the inertia dominant case, the bubble rising velocity is given by

$$v_g = k_1 \sqrt{gD}\,, \tag{13}$$

where k_1, g and D are the constant, the gravitational acceleration and the diameter of the pipe, respectively. The equation (13) represents the rising velocity independent of the viscosity of a liquid in the case that the inertia is dominat in the system. In the viscosity dominant case, the bubble rising velocity is given by

$$v_g = k_2 g D^2 (\rho_f/\mu_f)\,, \tag{14}$$

as an empirical equation, where μ_f and k_2 are the viscosity of a liquid and the constant, respectively.

WALLIS (1969) introduced three dimensionless parameters as mentioned above. One is the dimensionless inverse viscosity shown by

$$N_f = (\rho_f/\mu_f)\sqrt{gD^3} \tag{15}$$

and another is the Archimedes number shown by

$$N_{\mathrm{Ar}} = (1/\mu_f^2)\cdot(\sigma^3 \rho_f/g)^{1/2}\,, \tag{16}$$

where σ is the surface tension. The third one is termed the Eötvos number shown by

$$N_{\mathrm{Eö}} = gD^2\rho_f/\sigma\,. \tag{17}$$

The dominant cases of inertia, viscosity or surface tension were each arranged by means of the above dimensionless parameters as shown in Table 2, and the general case was discussed by WALLIS (1969) who termed the k_1 in Eq. (13) the dimensionless bubble velocity. The k_1 relative to the N_f in a slug flow is showh in Fig. 10. In the intermediate range of

Table 2. Three characteristic flows and their dimensionless groups (WALLIS, 1969).

Inertia dominant:	$N_f>300$, $N_{E\ddot{o}}>100 \rightarrow k_1=0.345$
Viscosity dominant:	$N_f<2$, $N_{E\ddot{o}}>100 \rightarrow k_1=0.01N_f$
Surface tension dominant:	$N_{E\ddot{o}}=3.37$, $N_f{}^2=6.2N_{Ar}$

*Dimensionless inversse viscosity

$$N_f=\frac{[D^3g(\rho_f-\rho_g)\rho_f]^{1/2}}{\mu_f}$$

*Archimedes number

$$N_{Ar}=\frac{\sigma^{3/2}\rho_f}{\mu_f{}^2g^{1/2}(\rho_f-\rho_g)^{1/2}}$$

*Eötvos number

$$N_{E\ddot{o}}=\frac{gD^2(\rho_f-\rho_g)}{\sigma}$$

N_f, 2 to 300, a good approximation for the dimensionless bubble velocity is made by

$$k_1=0.345(1-e^{-0.01N_f/0.345}). \quad (18)$$

In cases where the surface-tension effects are not negligible, the approximation is carried out by

$$k_1=0.345(1-e^{-0.01N_f/0.345})\times(1-e^{(3.37-N_{E\ddot{o}})/m}) \quad (19)$$

as a function of m which is constrained by N_f as follows:

$$\begin{aligned} 250<N_f &\quad ; m=10, \\ 18<N_f<250 &\quad ; m=69N_f, \\ N_f<18 &\quad ; m=25. \end{aligned} \quad (20)$$

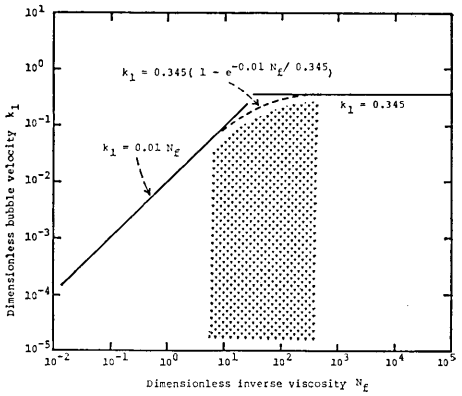

Fig. 10. Relationship between dimensionless inverse viscosity N_f and dimensionless bubble rising velocity v_g in slug flow (after WALLIS, 1969, Chap. 10, Fig. 10.4).

The rising velocity of a bubble in a stagnant and viscous liquid can be calculated by means of empirical equations (13) and (14), taken with $k_1=0.354$ (WALLIS, 1969, Eq. 10.18) and $k_2=0.01$ (WALLIS, 1969, Eq. 10.12), respectively. The results of the calculations are listed in Table 3. It cannot be said that the results from the empirical equations suit the data from the experiments. The reason is that the N_f's of our experiments are included in the intermediate range, 10^0 to 10^3, of the N_f in Fig. 10. Therefore, we should use Eq. (18) or Eq. (19). The result is also seen in

Table 3. It is found that our experimental data are universally arranged by the dimensionless bubble rising velocity in a slug-flow, given by Eq. (18). If we believe in the analogy in fluid dynamics relative to a slug-flow system, the analogy gives the bubble rising velocity in magmas.

Table 3. Bubble rising velocity by the empirical equations and from our experimental results (cm/sec).

μ_f (cs)	N_f	Empirical equations			Our experiment
		Eq. 13	Eq. 14	Eq. 18	
50	177.1		78.4	15.2	11—14
100	88.5		39.2	14.1	11—14
300	29.5	15.3	13.1	8.8	~8.5
500	17.7		7.8	6.1	~6.0
1000	8.9		3.9	3.8	~3.8

Our slug-flow model for a mechanism of successive eruptions as mentioned by IMAI (1983) can be supported by the experimental results, based upon N_f, according to the following part. Since Asama Volcano is an andesitic one, the density and the viscosity of the magma are assumed to be 2500 kg/m^3 and 10^4 to 10^5 poise by use of the physical properties of Mt. Hood Andesite (MURASE and MCBIRNEY, 1973), provided that the temperature of the magma is around 1150°C as presented by OOSHIMA (1976). The diameter of the volcanic conduct is considerd to range roughly from 5 to 10 meters. By using the above geophysical constants, the values of N_f are

Table 4. N_f as functions of viscosity and diameter of a pipe obtained by Eq. 15.

(a) density of magma=2500 kg/m^3

Diameter of conduit (m)	viscosity (poise) 10^4	10^5
5.0	87.5	8.8
10.0	247.5	24.8

(b) diameter of conduit=2.0 cm

viscosity (cs)	N_f
50	177.1
100	88.5
300	29.5
500	17.7
1000	8.9

calculated as listed in Table 4(a). The values of N_f in the present experiments are also seen in Table 4(b), on the basis of the physical properties of silicon oils and the inner diameter of pipe. Thus, both cases show a nearly similar variation in N_f as is also seen in Fig. 11.

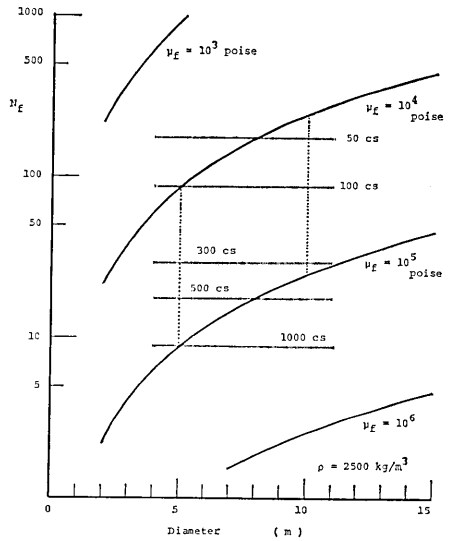

Fig. 11. General dimensionless representation of bubble rising velocity in slug flow based upon the dimensionless inverse viscosity (after WALLIS, 1969).

Table 5. Evaluation on bubble rising velocity in magmas based on N_f shown in Table 4(a).

N_f	velocity (m/sec)
8.75	0.54
24.75	1.24
87.5	2.22
247.5	2.41

The bubble rising velocity is evaluated from the N_f obtained from dynamical parameters that appeared in the model for mechanism of successive eruptions. The results of the evaluations bubble rising velocities are listed in Table 5. Conclusively, the bubble rises in viscous liquid, whose viscosity ranges from 10^4 to 10^5 poise, as a plug with a velocity in the range of 0.5 to 2.5 m/sec in the volcanic conduit whose diameter is taken to be 5 to 10 meters. If the above assumptions are valid, then the interval between the plugs is estimated to be within 150 meters based upon the time interval of successive eruptions, most of which occurred within 60 sec (SHIMOZURU *et al.*, 1975).

Moreover, it is found that the thickness of the liquid film becomes 0.2 to 0.35 times that of an inner radius of the cylindrical pipe, though the value is variable with the liquid viscosity. IMAI (1983) estimated the potential energy loss due to a liquid film flowing down along a valcanic conduit wall in order to interpret the seismic energy of implosion earthquakes associated with successive eruptions of Asama Volcano as mentioned previously. At the time of calculation on the energetics, the liquid film thickness was assumed to be one tenth of the inner diameter of volcanic conduit. According to our experimental results, however, the ratio of the liquid film thickness to the inner radius of pipe ranges roughly from 0.2

to 0.35 and the thickness namely becomes 0.1 and 0.18 times that of the inner diameter of pipe. Therefore, it is thought that the potential energy loss would be greater than those evaluated by IMAI (1983), with the result that the energetics would be more appropriate for the model.

6. Conclusion

To examine the validity of a model for the mechanism of successive eruptions proposed by IMAI (1983), one of the most basic experiments of two-phase flows is carried out by using several kinds of viscous liquids. In the present experiment, silicon oils whose viscosities are 50, 100, 300, 500 and 1000 cs and a cylindrical pipe whose inner diameter is 2.0 cm are used on the basis of N_f which supports the application of the present experimental results to the volcanological model. The film thickness of the magma was assumed to be 0.1 times the inner diameter of volcanic conduit in the model by IMAI (1983), whereas the thickness has been found to range from 0.1 to 0.18 times the inner diameter of pipe in the present experiment. Thus, the validity of the model has been further enhanced by the results of the experiment. The other basic results of the two-phase flows can be cited as follows. The rate of the decompressive expansion of a bubble becomes greater in relation to a lower viscosity of a liquid and the rate increases with the volume of the bubble regardless of liquid viscosity. The rising velocity of a bubble increases with a decrease in liquid viscosity. Moreover, the velocity of a larger bubble becomes more stable with an incease in liquid viscosity. It is believed that the above results would be of great value in interpreting volcanic phenomena.

Acknowledgements

The author wishes to thank Prof. D. Shimozuru, Prof. T. Watanabe, Mr. Kagiyama and Mr. Mikada of the University of Tokyo for their many suggestions on this study and Mr. T. Daikubara for making some parts of the experimental apparatus. He also wishes to thank the Hokutoriken Co. Ltd. for lending the pressure sensor and amplifier used in the present experiments without compensation. This papper is a part of a doctoral dissertation, Fac. of Sci., University of Tokyo, 1983.

References

IMAI, H., N. GYODA and E. KOYAMA, 1979, Explosion earthquakes associated with the 1973 eruptions of Asama Volcano. (Part I) Spectral studies, *Bull. Earthq. Res. Inst.*, 54, 161-186.

IMAI, H., 1980, Explosion earthquakes associated with the 1973 eruptions of Asama Volcano. (Part II) The summary of studies on explosion earthquakes and a model of explosive eruptions inferred from seismic data, *Bull. Earthq. Res. Inst.*, 55, 537-576.

IMAI, H., 1982, Implosion earthquakes associated with the 1973 eruptive activity of Asama Volcano, *Bull. Earthq. Res. Inst.*, 57, 303-315.

IMAI, H., 1983, A mechanism of successive eruption as inferred from seismic data associated with the 1973 eruptive stage of Asama Volcano, in *Arc Volcanism —Physics and Tectonics—*, 63-80, Ed. D. Shimozuru, and I. Yokoyama, Terrapub/Reidel, Tokyo.

MURASE, T. and A. R. MCBIRNEY, 1973, Properties of some common igneous rocks and their melts at high temperatures, *Bull. Geol. Soc. Am.*, 84, 3564-3592.

OOSHIMA, O., 1976, Fe-Ti oxide minerals of the 1973 eruption of Asama Volcano, *Sci. Papers Coll. Gem. Educ., Univ. Tokyo*, 26, 39-50.

SHIMOZURU, D., S. UTIBORI, N. GYODA, E. KOYAMA, T. MIYAZAKI, T. MATSUMOTO, N. OSADA and H. TERAO, 1975, The 1973 explosive activity of Asama Volcano. General description of volcanic and seismic events, *Bull. Earth. Res. Inst.*, 50, 115-151.

WALLIS, G. B., 1969, *One-dimensional two-phase flow*, McGrow-Hill, 408 pp.

WATANABE, M., 1976, On the sequence of seismic eruption at Asama Volcano, *Quarterly J. Seismol.*, 41, 1-11.

---

13. 1973年浅間火山に発生した断続微噴火に伴うImplosion地震に関する実験について

地震研究所　今井　博

1973年浅間火山噴火活動の際，2月16日から同月16日まで断続微噴火が発生した．個々の噴火に対応してImplosion地震と呼ばれる，浅間観測史上初めての噴火に伴う地震が筆者によって報告され，さらに気液二相流の概念を導入した断続微噴火の発生モデルが提出された．本報文では，そのモデルの妥当性を調べる目的で粘性流体を用いた基礎実験を行ない，その結果を報告した．用いた粘性流体はシリコン・オイルで，その粘性は50，100，300，500，1000センチストークスの5種類である．Wallisによって提唱されたN_fというパラメータに基づいて，用いた粘性流体の粘性が実際の火山火道内で起こる現象に対して適当であることが確められ，この実験結果の断続微噴火の発生モデルに対する有意性が保証された．その発生モデルに於て，Implosion地震のマグニチュードを説明するためのエネルギー論では火道壁とその中に存在する気泡との間に狭まれたマグマ液膜の厚さが重要であり，工学実験の結果に基づいて火道直径の1割と仮定された．本実験によれば，その液膜の厚さは火道半径の0.2～0.35（火道直径の0.1～0.18）倍になることが判明した．従って，断続微噴火の発生モデルにおけるマグマ液膜に対する仮定の妥当性が保証された．他に，基礎的データとして気泡の静水圧減少に伴う膨張速度及び気泡の上昇速度等が提出された．